Bulletin of Environment, Pharmacology and Life Sciences
Bull. Env. Pharmacol. Life Sci.[Spl. Issue 2] 2016: 139-151

Online ISSN 2277-1808
Journal's URL:http://www.bepls.com
CODEN: BEPLAD
Global Impact Factor 0.876
Universal Impact Factor 0.9804
http://doi-ds.org/doilink/05.2016-13212626/

Modeling Carbon Sequestration pattern of Casuarina plantation using RBFNN

G.Arulselvi
Department of Computer Science and Engineering,
Annamalai University, Annamalainagar, Tamilnadu, India

ABSTRACT
The Global warming forces countries in the world to pay efforts to reduce the amount of carbon emission. Perennial trees play an important role in terms of absorbing and storing carbon dioxide. Many studies indicated that carbon sequestration can be efficiently estimated via a method combining with forest inventories and remote sensing. In the present study, Therefore, the moderate resolution imaging specteroradioameter (MODIS) data are used to extract different kinds of vegetation indices. . The vegetation indices namely EVI (Enhanced Vegetation Index), GVMI (Global *vegetation Moiture index), TRVI (Total ratio vegetation index) and two radiation variables namely LST (Land surface temperature) and* $Albedo_{NIR}$ *are used to estimate the carbon sequestration potential of casuarina plantation of Cuddalore district of Tamilnadu, India. The improved remote sensing data based GPP model (IRS), which uses MODIS imagery derived three vegetation indices namely EVI, GVMI and TRVI and two radiation budget variables* $Albedo_{NIR}$ *and LST for the calculation of GPP usingIRS model. The same five features along with GPP is used as input parameter for training and testing the RBFNN. It classifies the pattern of carbon sequestration of casuarina plantation with an accuracy of 77.34%.*
Keywords: Casuarina, Gross primary production, Radialbasis function Neural Network, MODIS.

INTRODUCTION

Casuarina is an N-fixing needle leaf perennial tree that has been used extensively for windbreak and coastal stabilization in tropical and sub-tropical areas of the world The critical ecosystem services of coastal forests, including *Casuarina* plantations, have gained great recognition recently, particularly after the devastating 2004 Southeast Asian tsunami. It requires limited attention as it is a hardy plant which survives in harsh climate. *Casuarina* plantation has the potential to sequestrate atmospheric CO_2 and contributes to the regional C cycling. Most studies have focused on the ecological functions of *Casuarina*, such as land reclamation, windbreaks, erosion control, and wood and fuel production. However, the aboveground and belowground biomass increment and C sequestration in *Casuarina.* plantations are not estimated. Due to its large actual and potential planting areas in India and other parts of the world, the C sequestration potential in *Casuarina.* may greatly account for the regional and global C budget.

Comprehensive report on biomass and productivity of manmade plantations are available. However, information on carbon sequestrating potential of casuarinas is scanty, and the GPP estimation for large scale area of casuarina plantation using remote sensing data is not attempted. Hence, the present study was planned to establish the temporal dynamics of carbon sequestrating pattern of casuarina plantationin Cuddalore and Perambalur Districts of Tamilnadu, India using multispectral lremote sensing data.

The gross primary production (GPP) of an ecosystem represents the gross uptake of carbon dioxide (CO2) by vegetation for photosynthesis. It is the primary conduit of carbon flux from atmosphere to land and a key source of energy that fuels economies. On the other hand, CO2 from fossil fuel burning and ecosystem respiration is a major contributor to global warming or greenhouse effect. Fossil fuel burning has perturbed the carbon cycle, and affected the global climate, leading to worldwide research on climate change and the carbon cycle [Heinsch et al., 2006], [Urbanski et al., 2007]. However, considerable uncertainties still remain regarding the dynamics of carbon fluxes over both short and long time scales and effective strategies are necessary to acquire relevant information about carbon flux processes, to locate and to quantify terrestrial sources and sinks of carbon [Rahman et al., 2005].

As GPP is a measure of carbon uptake by vegetation, an improved knowledge about GPP can provide us a useful measure of the health of ecosystem and the global carbon cycle. Estimating GPP of terrestrial

ecosystems has been challenging because of its dependence on a variety of environmental factors [Mekela et al., 2008]. Among the existing methods, the light use efficiency (LUE) model proposed by Monteith has been widely used [Xiao et al., 2004], [Running et al., 2000], [Coops et al., 2005] to simulate the spatial and temporal dynamics of GPP because of its theoretical basis and practicality [Running et al., 2000]. LUE is defined as the amount of carbon uptake per unit of absorbed photo synthetically active radiation (APAR) by photosynthetic biomass. In LUE, it is assumed that

- the ecosystem GPP is directly related to amount of APAR and
- the actual LUE may be lesser than its theoretical value because of environmental stresses such as low temperatures or water deficits [Yuan et al., 2007].

The general form of LUE is:

$$GPP = \varepsilon \times FAPAR \times PAR \quad (1)$$

$$\varepsilon = \varepsilon_{max} \times F \quad (2)$$

Where PAR is the incident photo synthetically active radiation (MJ m^{-2}) per unit time, FPAR is the fraction of incident PAR absorbed by the canopy, max is the potential LUE (g C m^{-2} MJ^{-1}APAR) without environment stress, *F* is a scalar ranging from 0 to 1 representing the reduction of potential LUE under environmental stresses, *FPAR*× PAR gives the APAR and $\varepsilon_{max} \times F$ gives the realized LUE(Ɛ). In recent years, carbon fluxes measured by the eddy covariance (EC) tower sites set up over forest, grasslands, savannas, etc., has provides useful field measurements for us to parameterize and to validate GPP models. Furthermore, it has been shown that combining these EC tower measurements with remotely sensed (RS) data has the potential to enhance modeling of GPP based on LUE. The MODIS-GPP Algorithm [Running et al., 2004], Vegetation Photosynthesis Model [Xiao et al., 2004], EC-LUE [Yuan et al., 2007], etc., are some examples of successful application of remote sensing data in GPP modeling. The objective of this study is to develop a solely remote sensing data based GPP prediction model which does not depend on any supplementary meteorological data.

Recently developed remote sensing data based GPP prediction model, which does not depend on any supplementary meteorological data efficiently, calculate and the GPP in different forest ecosystem. [Jahan and Gan, 2009] developed the remotely sensed GPP model, using only on four remote sensing variables - two radiation budget variables ($Albedo_{NIR}$ and LST) and two ecosystem variables - Global vegetation moisture index (GVMI) and Enhanced vegetation index (EVI).

$$GPP = K \times GVMI^{a} \times LST^{b} \times Albedo_{NIR}^{c} \times EVI^{d} \quad (3)$$

Where *K* is a scalar, and *a, b, c, d* are exponents. The present study is taken up in semiarid casuarina plantation area, and hence, the remote sensing data based GPP prediction model was modified by adding an additional parameter called total ratio vegetation index (TRVI), which was specific for arid and semiarid vegetation. Several machine learning tools such as SVM, RBFNN and AANN have been used for pattern classification studies. The efficiency of this machine learning techniques varies with the nature of study and data available. The uses of these machine learning techniques in the carbon sequestration pattern studies are scanty. Hence, in the carbon sequestration pattern of casuarina plantation is classified using SVM, RBFNN and AANN. These classification tools utilize the vegetation indices calculated from the MODIS imagery.

MATERIALS AND METHODS

Study site and data sets

Study site

The study site is located in the casuarina plantation of Cuddalore and Perambalur Districts of Tamilnadu, India, and occupies an area of 50,000 *ha*. This area lies between11°15'N to 11°43'N latitude and 79°16'E to 79°44'E longitude and the elevation of the study area ranges from 5 to 65 MSL. The year is broadly divisible into two seasons: Dry season (March to September) and Wet season (October to February). Of the total annual rainfall 1012 *cm*, north east monsoon (October-December) accounts for75% of the rainfall and the remaining 25% of the rainfall occurs during January-September. The mean monthly maximum and minimum temperature ranges are 28 to44°C and 22-28°C respectively. The soil is sodic with sandy to salty clay loam texture characterised by unusually high pH (8.5-9.5) indicating poor water holding capacity to poor permeability.

Remotely sensed data:

For the study site, the 8-day surface reflectance data (MOD09A1, Collection 5) of the four spectral bands, blue, red, NIR (841-875 *nm*), and shortwave infrared (1628-1652 135 *nm*) were collected from 2007 to 2010 and then used to calculate vegetation indices - EVI and GVMI. The other 8-day composite MODIS

data sets used in this study include the 1 *km* LST (MOD11A2, collection 5) and 1 *km* GPP product(MOD17A2, Collection 5).
MOD11A2 is retrieved using the Split-Window algorithm and the thermal infra-redbands of MODIS [Wan and Dozier, 1996]. We also collected MODIS albedo product which is produced every 8 days with 16 days of acquisition. The Bidirectional Reflectance Distribution Function (BRDF) coefficients from MCD43A1 were used to calculate the actual albedo for the visible (VIS), NIR and shortwave bands (0.3- 0.7, 0.7-5.0, and 0.3-5.0μ *m*, respectively) as a function of optical depth, solar zenith angle, band ([Schaaf et al., 2002], http://daac.ornl.gov/MODIS/MODISmenu/ MCD43.html).
We estimated GPP with 1 *km* resolution which is same as that of MODIS GPP. Since the remotely sensed data are of 1 *km* (LST, MODIS GPP) and 500 *m* (reflectance and *albedo*) resolutions, for LST and MODIS GPP, we extracted digital values of a1-*km* pixel; while for reflectance and albedo, we used the average value of 2×2 pixels which represents the same $1km \times 1km$ area.

Research methodology

The research approach for casuarina plantation undertaken in this study can be summarized as follows:
1. Selecting EVI, GVMI, $Albedo_{NIR}$, LST and TRVI as the model predictors and investigating the relationships between these model predictors and GPP.
2. Calibrating GPP using IRS model for the year 2007-2010, and comparing its results with the MODIS GPP product (MODIS-17A2) and calculating the efficiency of RBFNN for classification of carbon sequestration pattern of casuarina plantation.

IRS-GPP model predictors

Global Vegetation Moisture Index GVMI:

Previous studies have demonstrated the possibility of using NIR and short wave infra-red bands to retrieve leaf and canopy water content (g/m^2) using Landsat – TM data [Hunl and Rock, 1989], hyperspectral data [Serrano et al.,, 2000], and VEGETATION (VGT) sensor data [Ceccato et al, 2001]. Recently, [Ceccato et al, 2002(a)], [Ceccato et al, 2002(b)] proposed to retrieve equivalent water thickness (EWT) at the canopy level using GVMI from the VGT sensor:

$$GVMI = \frac{(NIR+0.1)-(SWIR+0.02)}{(NIR+0.1)+(SWIR+0.002)} \quad (4)$$

where NIR and SWIR are reflectance of the rectified NIR band and short wave infrared bands, respectively. [Ceccato et al, 2002(a)] tested GVMI in retrieving EWT from four different ecosystems and found that water content retrieved from GVMI was consistent with field measured water content. Other studies also demonstrated the applicability of GVMI in retrieving EWT [Dansan and Bowyer, 2004], [Du et al., 2005]. To incorporate the effect of water stress in the R-GPP model, we used GVMI computed from MODIS reflectance products. In this study, we found that seasonal dynamics of GPP agrees well with GVMI (R^2=0.86) for the casuarinas plantation Fig. 1(b) and therefore GVMI is selected as a predictor.
When there is sufficient soil moisture (water is not a limiting factor), photosynthesis will probably depend more on temperature which is related to the incoming solar radiation. [Yuan et al., 2007] also reported that GPP is controlled either by air temperature or by soil moisture, whichever is the most limiting.

Near-infrared Albedo (*$Albedo_{NIR}$*):

Albedo (α), the fraction of incident solar radiation reflected by a surface plays a key role in partitioning the total radiative flux into absorbed, sensible, latent, and reflected fluxes [Bounoun et al., 2000]. The net radiation *Rn* is given as

$$R_n = \begin{cases} S_{in} - S_{out} + L_{in} - L_{out} \\ S_{in}(1-\alpha) + L_{in} - L_{out} \end{cases} \quad (5)$$

Where *Sin* and *Sout* are the incoming and outgoing solar (shortwave) radiation; *Lin* and *Lout* are the down welling and upwelling longwave radiation at the surface, respectively. *Albedo* influences the radiation absorbed by plant canopies and thereby affects physical and bio-geochemical processes such as photosynthesis, energy balance, evapotranspiration, and respiration [Wang et al., 2001], [Wang et al., 2002(a)], [Wang et al., 2002(b)].
Furthermore, surface albedo also affects rainfall, vegetation growth [Bounoua et al., 2000], [Wang and Davidson, 2007] and even droughts that could lead to desertification [Knorr et al., 2001]. The albedo of vegetation, unlike that of bare soil, shows temporal variability due to the seasonal behavior of plant

phenology such as green-up, peak greenness, drydown, and senescence. For example, Song [Song, 1998] found that the albedo of a wheat field decreased from the peak green to senescence stage.
Although some previous studies on GPP [Gebremichael and Barros, 2006], [Lchii et al., 2003] used albedo to calculate radiative fluxes, as far we know, none of them reported a direct relationship between NIR albedo and GPP, and most of these models used a constant albedo without considering its temporal variability.
In this study, albedo at the NIR band, $Albedo_{NIR}$(0.7 to 5μ m) has been used because the reflectance of vegetation is very strong at NIR band, and likely because of this reason, it is the most commonly used albedo in ecosystem modeling [Wang and Davidson, 2007], [Ghulami et al.,2007], [Ollingeri et al.,2008].
Since only 16-day resolution albedo data is available from MODIS, we have used that 16-day albedo product produced every 8 days (e.g., albedo of Date 1 corresponds to average albedo of day 1 to 16 while albedo of date 9 corresponds to average albedo of Date 9 to 24).To estimate the GPP of any 8 day period, we have used $Albedo_{NIR}$ averaged over that particular 8-day and the previous 8-day while the other predictors were averaged over that particular 8-day. For example, to calculate the average GPP of day 9 to 16(17 to 24), the average albedo of day 1 to 16 (9 to 24) is used while the other predictors were averages of day 9 to 16 (17 to 24). Therefore the R-GPP remains as an 8-dayGPP model.
Fig. 2(b) shows that the seasonal dynamics of $Albedo_{NIR}$ and GPP is strongly correlated with each other (R^2=0.82) and hence it was selected as a model predictor in IRS model. $Albedo_{NIR}$ gradually increases with the fresh of leaf formation because of the high reflectance of canopy leaves in the NIR band and continues until the peak green stage and then gradually decreases with the senescence of leaves is observed by Wang [Wang,2005] for a boreal deciduous forest of Saskatchewan, Canada.

Enhanced Vegetation Index (EVI):

EVI produces vegetation signal with improved vegetation monitoring through canopy background and atmospheric corrections [Waring et al.,2006] as shown in Equation 6. It is more sensitive than the popular normalized difference vegetation index (NDVI) in high biomass regions. EVI has been shown to be a good predictor of growing season GPP for many sites and it was used as a predictor in some previous models [Xiao et al., 2004]. In this study we found that the seasonal dynamics of GPP agrees reasonably well with EVI (R^2=0.84) for the casuarina plantation Fig. 1(a) and shows that EVI is selected as a predictor.

$$EVI = G\frac{NIR-RED}{NIR+C_1RED-C_2B+L} \tag{6}$$

Land Surface Temperature (LST):

LST is a potential predictor for GPP estimation because it can incorporate the effect of temperature and Vapor pressure density (VPD) on vegetation [Hashimoto et al.,2008]. It is highly correlated with vegetation dynamics [Sun and Kafatos,2007] and is positively correlated with NDVI in high latitudes ([Karnieli et al.,2006]). The slope of LST/NDVI to be related to the evapotranspiration of Soil. Some studies [Yuan et al., 2007], [Sims et al., 2008] reported that photosynthesisis predominantly controlled by temperature only at the beginning and the end of a growing season, but by moisture conditions throughout the growing season. Therefore we used a scaled LST (LSTs) (equ.7) to set GPP to zero when LST is below 0^{o}C.

$$LST_s = \begin{cases} \frac{LST}{LST_{max}}; & when\ LST > 0\,^{\circ}C \\ 0; & when\ LST \leq 0\,^{\circ}C \end{cases} \tag{7}$$

where LST is the observed LST and LST*max* is the maximum LST. In this study LST*max* is set to 45^{o}C. Fig. 3(a) shows that GPP is strongly correlated with LSTs(R^2=0.71). From January to April, GPP increases with increasing LSTs; beyond that it decreases up to July due to high temperature and leaf senescence. The LST start increases again from July due to the onset of southwest monsoon as shown in Fig. 3(a). However, it is also found that GPP does not respond instantaneously to temperature rise during the early growing season. Furthermore, low LSTs during the start and the end of each growing year restricts water and nutrient uptake, and hence, it affects photosynthesis [Sims et al., 2008].

Total ratio vegetation index (TRVI):

In arid and semi-arid regions, soil background has more reflectance in the nearinfrared (NIR) and red (RED) wavelengths of vegetation. Soil components that affect spectral reflection include colour, roughness and water content. Roughness also hasthe effect of decreasing reflectance because of an increase in multiple scattering and shading. RED-NIR scatter diagrams, termed the 'soil line', are used as a reference point in most vegetation studies.
The problem is that real soil surface is not homogeneous and composite of several types. Analysis has shown that for a given soil characteristics, variability in one wavelength is often functionally related to

reflectance in another wavelength. Vegetation over is usually sparse compared to soil background and soil and plant spectral signatures tend to mix non-linearly.
Thus, arid plants tend to lack the strong red edge found in plants of humid regions due to ecological adaptations to the hot desert environment. It is decided to introduce the new vegetation index based on total wavelength (visible and NIR) in the GPP calculation. The total ratio vegetation index (TRVI) is the ratio of NIR and the sumof visible and NIR wavelengths and is calculated using the following equation

$$TRVI = 4\left[\frac{NIR-RED}{NIR+RED+GR+B}\right] \quad (8)$$

where RED and NIR stands for spectral measurement acquired in the red and near infrared regions, respectively.
For this equation, the normalized difference is divided by the total of visible and near infrared wavelengths. In this equation "4" is the measured reflectance. In fact this equation shows the ratio of the normalized difference of reflectance and measured reflectance of all bands (i.e) the four bands in the multispectral image. [HadiFadaei et al., 2012] used TRV Ito estimate the stand density of vegetation.
Fig. 2(a) shows that seasonal dynamics of TRVI and GPP is strongly correlated with each other (R^2=0.88) and hence TRVI is selected as a model predictor in the present study.

IRS-GPP model development and results

Given that GVMI, EVI, TRVI, $Albedo_{NIR}$ and LSTs are correlated to GPP, we propose remotely sensed GPP (IRS-GPP) model (9) based on these five RS predictors only,

$$GPP = K \times GVMI^a \times LST^b \times Albedo_{NIR}^c \times EVI^d \times TRVI^e \quad (9)$$

Where *k* is a scalar, and *a, b, c, d* and *e* are exponents. These model parameters were calculated using the MODIS data for the study site and a nonlinear optimization scheme, the Generalized Reduced Gradient (GRG2)[Spaulding, 1998]. By GRG2, the optimized values of *k, a, b, c, d, e* have been found to be 114, 0.885, 1.05, 0.695, 0.933and 0.01 respectively.

RESULTS AND DISCUSSION

Seasonal dynamics of EVI from eight-day composites of MODIS

The performance of MODIS, EVI changed significantly over time, reaching its peak in early summer and then declining gradually. In the present study the EVI of the casuarina plantation ranged from 0.2 to 0.78, the maximum EVI was noticed in the month of January and the lowest EVI was observed in the peak summer (May) as shown in Fig. 1.
The temporal dynamics of EVI within the plant-growing season is closely correlated to the dynamics of observed GPP. EVI is sensitive to phenological changes in leaf and canopy, and the other factor which affects the EVI is change in photosynthetic active vegetation and non-photosynthetic vegetation proportions within individual leaves (leaflevel), and age of the leaves.
Evergreen needle leaf vegetation consist of leaves with various ages of years. As a needle leaf get old, it changes its size (leaf thickness), dry weight and chlorophyll content. Based on a comparative assessment of needle anatomy of red spruce needle leaf thickness of 1*st* year leaves is about 1% smaller than that of 2*nd* year leaves and there is less intracellular air space in the 2*nd* year leaves .
Although chlorophyll concentration may be stable over the seasons, an increase in leaf thickness results in a larger volume of needle leaf, which lead to dilution effect of chlorophyll in the needle leaf. The changes in the leaf size (thickness), intercellular air space, dry weight and distribution effect might together affect reflectance, transmittance and absorption of PAR by needle leaf, for instance, the 2*nd* year needle leaf have slightly higher reflectance value in the blue band, but little changes of reflectance values in red band in comparison to first year needles. After reaching the peak in early summer, NIR values decline gradually resulting in low EVI value.

Seasonal dynamics of GVMI from eight-day composites of MODIS

The GVMI has distinct seasonal dynamics over the year as shown in Fig. 1(b). High GVMI values in winter and early spring are attributed to increased availability of soil moisture in soil. During the winter and early spring, plant can extract ample quantity of water for its growth, resulting in higher leaf water content. This might be the reason for the high GVMI value during the winter and early spring seasons. As the summer approaches the GVMI starts decreasing due to the reduction in leaf moisture content and leaf maturity. Jahan and Gan[Jahan and Gan, 2011] have established the positive relationship between leaf moisture content and GVMI.

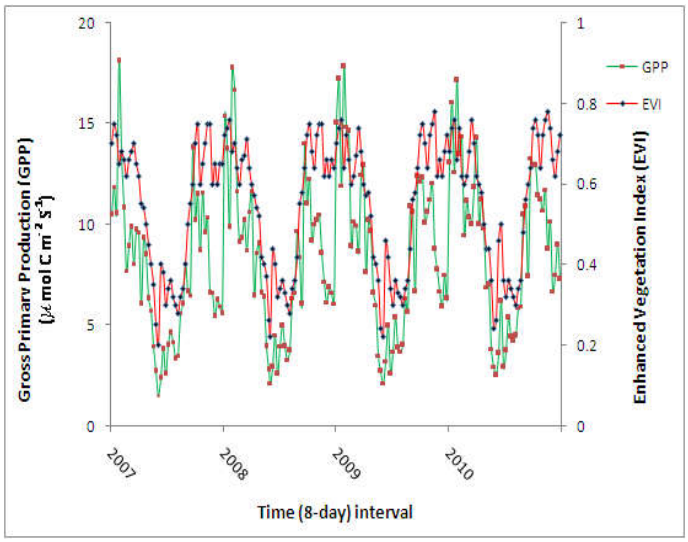

(a)

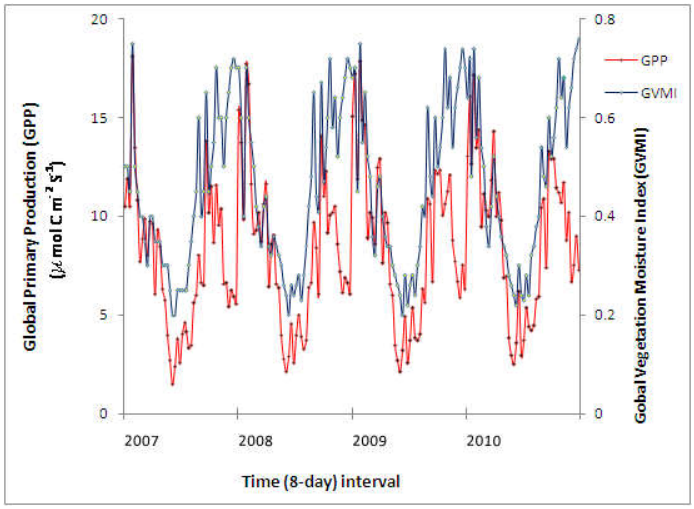

(b)

Fig. 1: Seasonal Dynamics of (a) Enahanced vegetation index (EVI) with GPP. (b) Global vegetation moisture index (GVMI) with GPP.

Seasonal dynamics of TRVI from eight-day composites of MODIS

Changes in the value of TRVI during the plant growing season is depicted are Fig. 2.In the present study, the TRVI ranged from 0.12 to 0.3, and maximum TRVI is recorded in the month of January. TRVI is also affected by leaf moisture and plant growing season. As the soil moisture declines from January to June, the TRVI also decreases considerably. Vegetation that is dead or stressed reflects more red light and less NIR light. This might be the reason for low TRVI during summer (May-June). Similarly the TRVI increases as the new leaves are formed, this was clearly noticed in the study from the month of July to December, which coincides with the onset of monsoon rainfall. The lowest TRVI was observed in the month of May-June. A positive correlation(0.84) was noticed between TRVI and GPP.

The present study is conducted in semiarid region. Generally in semi arid region, the green vegetation index tends to decrease with low reflecting soil background and the influence of soil background has been found to seriously hamper the assessment and characterisation of vegetation canopy cover [Huete and Jackson, 1987]. Use of this TRVI in the IRS model might have reduced the impact of reflection from soil background.

Seasonal dynamics of Albedo (Albedo$_{NIR}$) from eight day composites of MODIS

Reflectance of vegetation is very strong at NIR band and likely because of this reason, it is most commonly used in ecosystem modeling. In the present study, the albedo value ranged from 0.14 to 0.3. As that of EVI, and GVMI, albedo value also increased during the new flush formation and in early spring season. The maximum albedo(0.3)was noticed in the month of February and started declining during summer as shown in Fig. 2(b). The lower albedo value of (0.14) was noticed in the month of May. From the month of

June onwards, Albedo$_{NIR}$ gradually increased with the green up of leaves due to the onset of south west monsoon, high reflectance of canopy leaves in NIR band continued until the peak green stage and then gradually decreased with the senasence of leaves as it was observed by Wang [Wang,2005] for boreal deciduous forest of Canada.

Seasonal dynamics of LST from eight-day composites of MODIS

Temperature is an important factor which directly influences the photosynthesis and GPP. In this study the LST ranged from 0.25 to 0.8, from the month of January to April. The LST increased gradually and reached the peak value in the month of May and then declined. The GPP*obs* increased with increase in LST till April, beyond that GPP decreased as the LST increased. Again from the month of June, LST started declining whereas GPP increased gradually as shown in Fig. 3(a).

Predicted gross primary production from eight-day composites of MODIS

The results from simulations of the IRS model using eight-day composite MODIS data have shown that the IRS model predicts reasonably well the gross primary production of a casuarina plantation. The IRS model overestimated GPP as compared to MODISGPP as indicated by the slopes of simple linear regression models between IRS model predicted GPP and MODIS GPP as shown in Fig. 3(b). IRS GPP*pred* (from eight day MODIS composites) was only slightly larger (5%) than MODIS GPP. Performance of all models depends upon input data.

For the IRS model, it is largely vegetation indices from eight-day MODIS imagery that affect performance of IRS model. In comparison to other PEM models that employ only NDVI [Running et al., 2000], the IRS model has three simple but innovative features. The first feature is that the IRS model uses an improved vegetation index that is related to vegetation greenness (EVI). The second feature is that the IRS model uses an improved vegetation index that is related to vegetation water content (GVMI) to estimate the effect of water on photosynthesis and the third important feature is vegetation index related to arid and semiarid vegetation (TRVI), which minimize the soil background reflection in the GPP model.

One advantage of using water-related vegetation index in the IRS model is that there is no need for a soil moisture model that is usually driven by very coarse resolution of input datasets (e.g., precipitation, soil texture, and soil depth), which could result in large uncertainty or error in soil moisture.

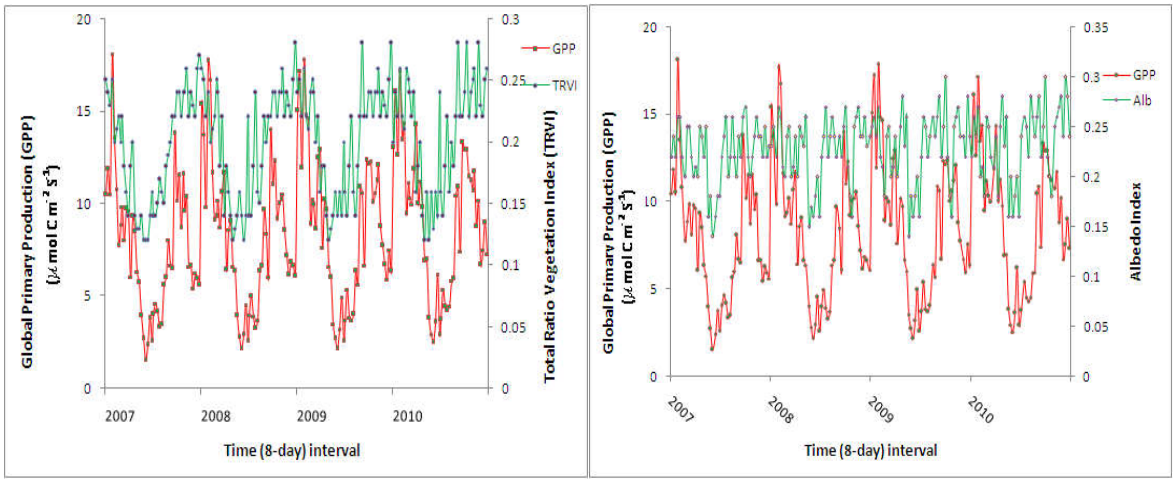

(a) **(b)**

Fig. 2: Seasonal Dynamics of (a) Total ratio vegetation index (TRVI) with GPP. (b) Albedo index with GPP.

There exist a few water-oriented vegetation indices [Ceccato et al, 2002(a)],[Xiao et al., 2002], [Maki et al., 2004], and extensive field work is needed to collect seasonal data of leaf and canopy water content, which would help to evaluate those spectral water indices and improve understanding of water-related biophysical processes of leaves over time. In addition, a comparison between water-related vegetation index and soil moisture data from a soil moisture model should be conducted. Although these two innovative features need to be validated across various biomes through systematic and extensive field measurement and radiative transfer modeling, the IRS model has the potential to improve estimation of seasonal dynamics and interannual variations of gross primary production of arid and semiarid perennial vegetation, in comparison to the other existing PEM models that employ NDVI only.

The IRS model uses the new vegetation index, the total ratio vegetation indexwhich is developed specifically for the arid and semiarid regions to minimize the soilbackground reflection.

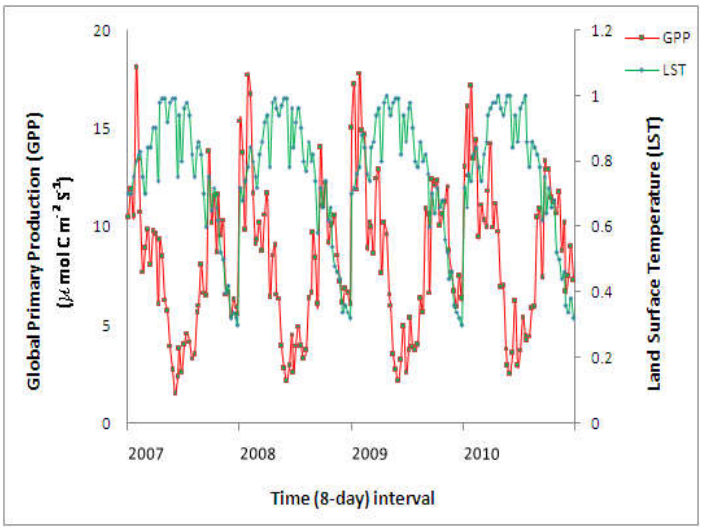

(a)

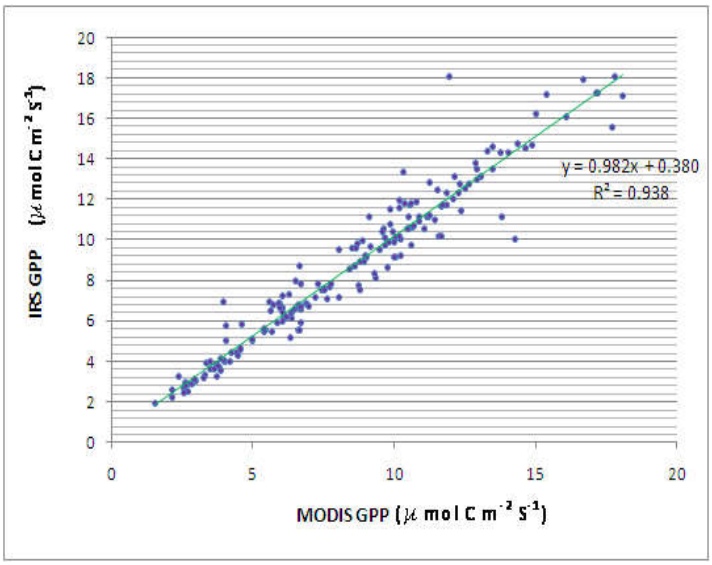

(b)

Fig. 3: (a) Seasonal Dynamics of LST and GPP. (b) Comparison of IRS GPP with MODIS GPP.

Classification Technique

Radial Basis Function Neural Network

The Radial Basis Function Neural Network (RBFNN) [Haykin, 2001] has a feed forward architecturewith an input layer, a hidden layer, and an output layer as shown in Fig. 4.Radial basis functions are embedded into a two-layer feed forward neural network. Such a network is characterized by a set of inputs and a set of outputs. In betweenthe inputs and outputs, there is a layer of processing units called hidden units.

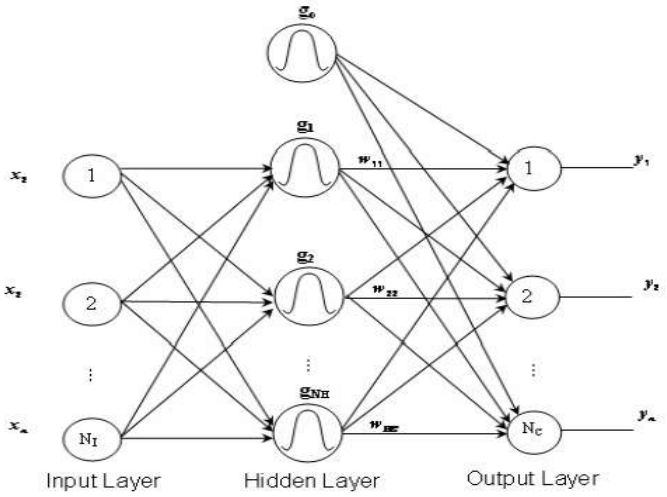

Fig. 4: Radial basis function neural networks.

Eachof them implements a radial basis function. The input layer of this network has $n_i$units for a $n_i$dimensional input vector. The input units are fully connected to the$n_h$hidden layer units, which are in turn fully connected to the $n_c$output layer units,wheren_c is the number of output classes. The activation functions of the hidden layerare chosen to be Gaussians [Koh et al., 2002], and are characterized by their mean vectors (centers)μ_i, and covariance matrices C_i,$i = 1, 2, \cdots n_h$,. For simplicity, it is assumed that thecovariance matrices are of the form$C_i = \sigma_i^2 I, i = 1,2, \ldots, n_h$. Then the activation function of the i^{th} hidden unit for an input vector $x_j$is given by

$$g_i(x_j) = exp\left(\frac{-\|x_j-\mu_i\|^2}{2\sigma_i^2}\right) \quad (10)$$

The $\mu_i$and$\sigma_i^2$are calculated by using suitable clustering algorithm. Here the *k*-means clustering algorithm is employed to determine the centers. The algorithm is composed of the following steps:

1. Randomly initialize the samples to *k* means (clusters) $\mu_1, \ldots, \mu_k$
2. Classify n samples according to nearest μ_k.
3. Recomputed μ_k.
4. Repeat the steps 2 and 3 until no change in μ_k.

The number of activation functions in the network and their spread influence the smoothness of the mapping. The assumption $\sigma_i^2 = \sigma^2$ is made to ensure that the activation functions are not too peaked or too flat where σ^2 is given by

$$\sigma^2 = \frac{\eta d^2}{2} \quad (11)$$

In the above equation, *d* is the maximum distance between the chosen centers, and η is an empirical scale factor which serves to control the smoothness of the mapping function. Therefore, the above equation is written as

$$g_i(x_j) = exp\left(\frac{-\|x_j-\mu_i\|^2}{\eta d^2}\right) \quad (12)$$

The hidden layer units are fully connected to the n_c output layer units through weights w_{ik}. The output units are linear, and the response of the k_{th} output unit for an input $\boldsymbol{x_j}$ is given by

$$y_k(x_j) = \sum_{i=0}^{n_h} w_{ik} g_i(x_j), k = 1, 2, \ldots, n_c \quad (13)$$

where$g_0(x_j)$ = 1. Given n_t samples from n_c classes, training the RBFNN involves estimating $\mu_i, i = 1,2, \ldots, n_h, \eta, d^2, and\ w_{ik}, i = 0,1,2, \ldots, n_h, k = 1,2, \ldots, n_c$.

.

Classification of casuarina plantation using RBFNN

Six features were extracted using MODIS imagery at the rate of four per month from 2007-2010. So altogether 184 samples were obtained. For RBFNN training, 164 samples were taken out of 184, each with 6 features are given as input to the RBFNN model. The RBF centers are located using k-means

algorithm. The weights are determined using least squares algorithm. The value of k = 2, 3, 4 and 5has been used in our studies. The system gives optimal performance for k = 4. For training, the weight matrix is calculated using the least squares algorithm.

For classification, the feature vectors are extracted and each of the feature vectors is given as input to the RBFNN model. The average output is calculated for each of the output neurons. The class to which the each sample belongs is decided based on the highest confidence score. The performance measures calculated for the three different classes such as class 0 , class 1 and class 2 are shown in Table 1.

The classwise performance of RBFNN for carbon sequestration pattern classification of casuarina plantation using satellite imagery derived vegetation indices (MODIS)are given in Table 1 and Fig. 5(c). The results of the analysis showed that increase in the number of clusters increase the sensitivity, precision, F-score and accuracy. However, some variation was observed with specificity.

Sensitivity: Increase in cluster number from 2 to 4 increase the sensitivity from83.00% to 97% in class 0 and 86% to 92% in class 1. However, a declining trend insensitivity was observed with cluster 5 in both class 0 and class 1. In class 2 increase in number of clusters from 2 to 5 increased the sensitivity value from 71% to 89%.

Specificity: No clear trend was observed with specificity. Increase in the number of cluster from 2 to 3 increased the specificity from 14% to 33%, further increase in number of clusters decreased the specificity in class 0. In class 1, increase in specificity was noticed with increase in number of clusters from 2 to 3 and a declining trend was noticed with cluster 3 (9%) and in cluster 4 specificity increased to 25%. No clear trend was noticed in class 2 in respect of specificity.

Precision: The precision value increased with increased number of clusters from2 to 4 in all the three classes. Increase in the cluster number from 2 to 4 increased the precision value from 68% to 78% in class 0, 67% to 75% in class 1 and 73% to 79% in class 2. Increase in cluster from 4 to 5 decreased the precision value.

F-score and Accuracy: A very similar trend as that of precision was noticed with F-score and accuracy. Increase in the cluster number from 2 to 4 increased the both F-score and accuracy.

Increase in F-score and accuracy from 75% to 86% and 61% to 77% was noticed in class 0 as the in cluster increased from 2 to 4. Similarly in class 1 and class 2 F-score increased from 75% to 83% and 72% to 83% respectively. Accuracy also increased with increase in cluster from 2 to 5. The increase in accuracy was from 62% to 72%in class 1. The increased accuracy of 60% to 74% was noticed with increase in cluster number from 2 to 4 in class 2.

Increase in the cluster number from 2 to 4 increased the sensitivity, precision and average accuracy. However the highest the specificity (28%) was noticed with cluster 3.The cluster 2 recorded the lowest value in respect of sensitivity, specificity, precision and average accuracy. Fig. 5 shows that the performance of RBFNN for carbon sequestration classification is 77.34%.

Table 1: Class-wise performance of RBFNN for carbon sequestration pattern classification of casuarina plantation using satellite imagery derived vegetation indices(MODIS).

Class	Clusters	Sensitivity (%)	Specificity (%)	Precision (%)	F-Score (%)	Accuracy (%)
0	2	83.00	14.00	68.00	75.00	61.00
	3	93.00	33.00	73.00	82.00	73.00
	4	97.00	18.00	78.00	86.00	77.00
	5	94.00	10.00	76.00	84.00	73.00
1	2	86.00	14.00	67.00	75.00	62.00
	3	90.00	30.00	74.00	81.00	71.00
	4	92.00	09.00	75.00	83.00	71.00
	5	89.00	25.00	76.00	82.00	72.00
2	2	71.00	33.00	73.00	72.00	60.00
	3	76.00	20.00	71.00	73.00	60.00
	4	87.00	36.00	79.00	83.00	74.00
	5	89.00	27.00	76.00	82.00	72.00

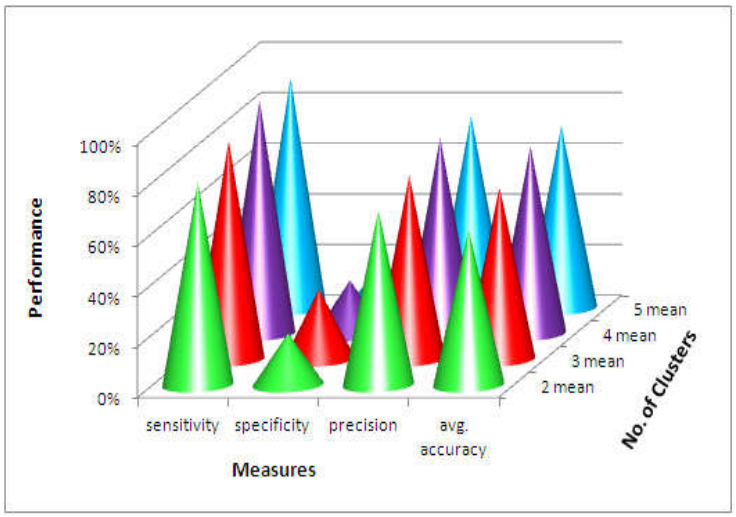

(a)

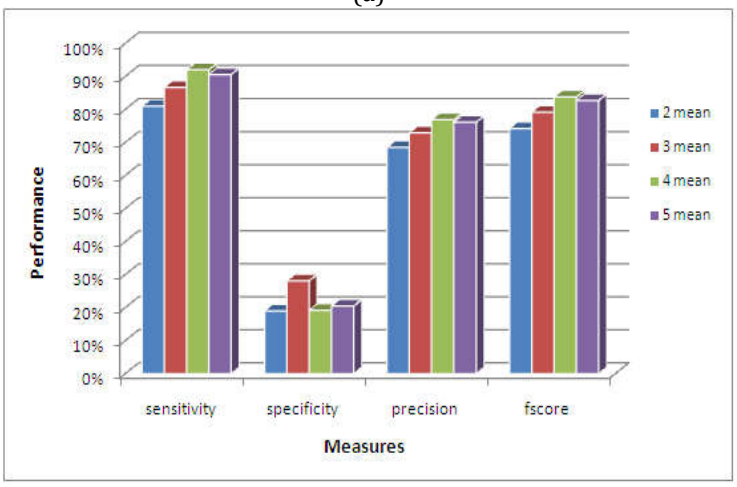

(b)

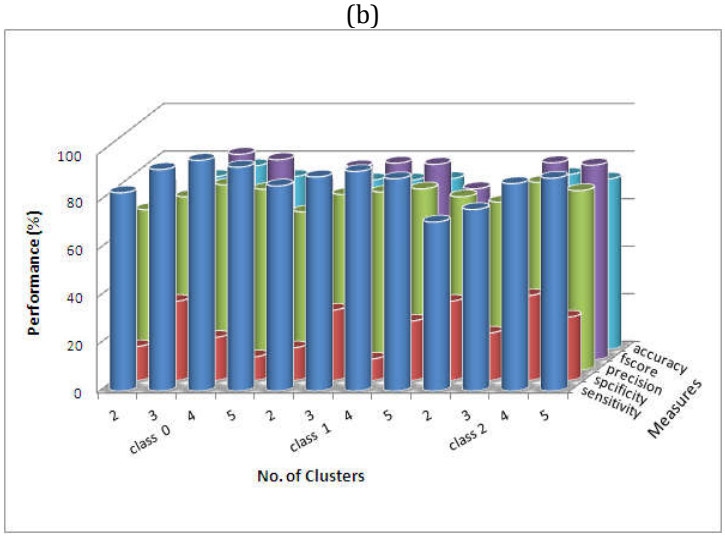

(c)

Fig. 5: (a)Average performance of RBFNN for different means for each class. (b)Performance of RBFNN for different means for all classes. (c) Overall performance of RBFNN for each mean in Casuarina plantation.

CONCLUSION

In this study, an improved remote sensing data based GPP model (IRS), which uses MODIS imagery derived three vegetation indices namely EVI, GVMI and TRVI and two radiation budget variables $Albedo_{NIR}$ and LST for the calculation of GPP using IRS model. The same five features along with GPP is

used as input parameter for training and testing the RBFNN. It classifies the pattern of carbon sequestration of casuarina plantation with an accuracy of 77.34%.

REFERENCES

1. G. Arulselvi, Pattern Classification Techniques for Analzing Carbon Sequestration from satellite images, Ph.D. thesis, Department of Computer Science and Engg., Annamalai University, Chidambaram, 2012.
2. L. Bounoua, G. J. Collatz, S. O. Los, P. J. Sellers, D. A. Dazilich, C. J. Tucker, and D. A. Randall, "Sensitivity of climate to changes in NDVI," *J. of Climate*, vol. 13, pp. 2277–2292, 2000.
3. P. Ceccato, S. Flasse, S. Tarantola, S. Jacquemoud, and J. M. Gregoire, "Detecting vegetation leaf water content using reflectance in the optical domain," *Remote Sensing of Environment*, vol. 77, pp. 22–33, 2001.
4. P. Ceccato, S. Flasse, S. Tarantola, S. Jacquemoud, and J. M. Gregoire, "Detecting vegetation leaf water content using reflectance in the optical domain," *Remote Sensing of Environment*, vol. 77, pp. 22–33, 2001.
5. P. Ceccato, S. Flasse, and J. M. Gregoire, "Designing a spectral index to estimate vegetation water content from remote sensing data part 2. validation and applications," *Remote Sensing of Environment*, vol. 82, pp. 198–207, 2002(a).
6. P. Ceccato, N. Gobron, S. Flasse, B. Pinty, and S. Tarantola, "Designing a spectral index to estimate vegetation water content from remote sensing data: Part 1 theoretical approach.," *Remote Sensing of Environment*, vol. 82, pp. 188–197, 2002(b).
7. N. C. Coops, R. H. Waring, and B. E. Law, "Assessing the past and future distribution and productivity of ponderosa pine in the pacific northwest using a process model, 3-PG," *Ecological Modelling*, vol. 183, pp. 107–124, 2005.
8. F. M. Danson and P. Bowyer, "Estimating live fuel moisture content from remotely sensed reflectance," *Remote Sensing of Environment*, vol. 92, pp. 30–321, 2004.
9. X. Du, S. Wang, and Y. Zhou, "Monitoring and spatio-temporal evolution researching on vegetation leaf water in china," vol. 4, pp. 2365–2368, 2005.
10. R.O. Duda, P.E. Hart, and D.G. Stork, *Pattern Classification*, John Wiley & Sons, Singapore, 2003,.
11. M. Gebremichael and E. P. Barros, "Evaluation of MODIS gross primary productivity (GPP) in tropical monsoon region," *Remote Sensing of Environment*, vol. 100, pp. 150–166, 2006.
12. Ghulam, Q. Qin, and Z. Zhan, "Designing of the perpendicular drought index,"*Remote Sensing of Environment*, vol. 52, pp. 1045–1052, 2007.
13. HadiFadaei, Rikie Suzuki, Tetsuro Sakai, and Kiyoshi Torii, "A proposed new vegetation index, the total ratio vegetation index (TRVI), for arid and semi-arid regions," *International Archives Photogrammetry, Remote Sensing and Spatial Information Sciences*, vol. XXXIX-B8, 2012.
14. H. Hashimoto, J. L. Dungan, M. A. White, F. Yang, A. R. Michaelis, S. W. Running, and R. R. Nemani, "Satellite-based estimation of surface vapor pressure deficits using MODIS land surface temperature data," *Remote Sensing of Environment*, vol. 112, pp. 142–155, 2008.
15. F. A. Heinsch, M. Zhao, S. W. Running, J. S. Kimball, R. R. Nemani, K. J. Davis, P. V. Bolstad, B. D. Cook, A. R. Desai, D. M. Ricciuto, B. E. Law, W. C. Oechel, H. Kwon, H. Luo, S. C. Wofsy A. L. Dunn, J. W. Munger, D. D. Baldocchi, L. Xu, D. Y. Hollinger, A. D. Richardson, P. C. Stoy, M. B. S. Siqueira, R. K. Monson, S. P. Burns, and L. B. Flanagan, "Evaluation of remote sensing based terrestrial production from MODIS using AmeriFlux eddy tower flux network observations," *IEEE Trans. Geosci. Remote Sens.*, vol. 44, pp. 1908–1925, 2006.
16. S. Haykin, *Neural Networks: A Comprehensive Foundation*, Pearson Education, Singapore, 2001.
17. R. Huete and R. D. Jackson, "Suitability of spectral indices for evaluating vegetation characterstics on arid range lands," *Remote Sensing of Environment*, vol. 25, pp. 89–105, 1987.
18. N. Jahan and T. Y. Gan, "Modeling gross primary production of deciduous forest using remotely sensed radiation and ecosystem variables," *Journal of Geophysical Research*, vol. 114, pp. G04026, 2009.
19. N. Jahan and T. Y. Gan, "Modeling vegetation-climate relationship in a central mixed wood forest region of Alberta using normalized difference and enhanced vegetation indices," *Journal of Geophysical Research*, vol. 32, pp. 313–335, 2011.
20. Karnieli, M. Bayasgalan, Y. Bayasgalan, N. Agam, S. Khudulmur, and C. J. Tucker, "Comments on the use of the vegetation health index over Mongolia," *Int. J. remote sensing*, vol. 27, pp. 2017– 2024, 2006.
21. W. Knorr, K. G. Schnitzler, and Y. Govaerts, "The role of bright desert regions in shaping North African climate," *Geophys. Res. Lett.*, vol. 28, pp. 3489–3492, 2001.
22. L.H. Koh, S. Ranganath, and Y.V. Venkatesh, "An integrated automatic face detection and recognition system," *Pattern Recognition*, vol. 35, pp. 1259–1273, 2002.
23. K. Lchii, Y. Matsui, K. Murakami, T. Mukai, Y. Yamguchi, and K. Ogawa, "A simple global carbon and energy coupled cycled model for global warming sisimulation: sensitivity to the light saturation effect," *Tellus*, vol. 55, pp. 676–691, 2003.
24. Makela, M. Pulkkinen, P. Kolari, F. Lagergren, P. A. Lindroth, D. Loustau, E. Nikinmaa, T. Vesala, and P. Hari, "Developing an empirical model of standard GPP with the LUE approach: analysis of eddy covariance data at five contrasting coniferous sites in Europe," *Global Change Biol.*, vol. 14, pp. 92–108, 2008.
25. M. Maki, M. Ishiahra, and M. Tamura, "Estimation of leaf water status to monitor the risk of forest fires by using remotely sensed data," *Remote Sensing of Environment*, vol. 90, pp. 441–450, 2004.
26. S. V. Ollinger, A. D. Richardson, M. E. Martin, D. Y. Hollinger, S. E. Frolking, P. B. Reich, L. C. Plourde, G. G. Katul, J. W. Munger, R. Oren, M. L. Smith, K. T. Paw, P. V. Bolstad, B. D. Cook, M. C. Day, T. A. Martin, R. K. Monson, and H. P.

Schmid, "Canopy nitrogen, carbon assimilation, and albedo in temperate and boreal forest: Functional relations and potential climate feedbacks," *PNAS.*, vol. 105, pp. 19366–19341, 2008.
27. K. S. Parihar and B. S. Rana, "Management practices in agroforestry," *In: Technical report on Biennial workshop on All India Coordinated Research Project on Agroforestry. (I.C.A.R)*, pp. 40–44, Mar. 1999.
28. F. Rahman, D. A. Sims, V. D. Cordova, and B. Z. El-Masri, "Potential of MODIS EVI and surface temperature for directly estimating per-pixel ecosystem C fluxes," *Geophys. Res. Lett.*, vol. 32, no. L19404, pp. doi:10.1029/2005GL024127, 2005.
29. Ruimy, G. Dedieu, and B. Saugier, "TURC: a diagnostic model of continental gross primary productivity and net primary productivity," *Global Biogeochemical Cycles*, vol. 10, pp. 269–285, 1996.
30. S. W. Running, P. E. Thornton, R. Nemani, and J. M. Glassy, "Global terrestrial gross and net primary productivity from the Earth Observing system. In O. E. Sala, R. B. Jackson, H. A. Mooney and R. W. Howarth (Eds.)," pp. 44–57, 2000.
31. S. W. Running, R. R. Nemani, F. A. Heinsch, M. Zhao, M. Reeves, and H. Hashimoto, "A continuous satellite-derived measure of global terrestrial primary production," *Bioscience*, vol. 54, pp. 547–560, 2004.
32. B. Schaaf, F. Gao, A. H. Strahler, W. Lucht, X. Li, T. Tsang, N. C. Strugnell, X. Zhang, Y. Jin, J. P. Muller, P. Lewis, M. Barnsley, P. Hobson, M. Disney, G. Roberts, M. Dunderdale, C. Doll, R. d'Entermont, B. Hu, S. Liang, J. Privette, and D. Roy, "First operational BRDF, albedo nadir reflectance products from MODIS," *Remote Sensing of Environment*, vol. 83, pp. 135–148, 2002.
33. L. Serrano, J. A. Gamon, and J. Penuelas, "Estimation of canopy photosynthetic and nonphotosynthetic components from spectral transmittance," *Ecologi*, vol. 81, pp. 3149– 3162, 2000.
34. A. Sims, A. F. Rahman, V. D. Cordova, B. Z. El-Masri, D. D. Baldocchi, L. B. Flanagan, A. H. Goldstein, D. Y. Hollinger, L. Misson, R. K. Monson, W. C. Oechel, H. P. Schimd, S. C. Wofsy, and L. Xu, "A new model of gross primary productivity for North American ecosystems based solely on the enhanced vegetation index and land surface temperature from MODIS," *Remote Sensing of Environment*, vol. 112, pp. 1633–1644, 2008.
35. J. Song, "Diurnal asymmetry in surface albedo," *Agricultural and Forest Meteorology*, vol. 92, pp. 181–189, 1998.
36. K. A. Spaulding, "Neural metamorphic optimization algorithms," 1998.
37. Sun and M. Kafatos, "Note on the NDVI-LST relationship and the use of temperature related drought indices over north America," *Geophys. Res. Lett.*, vol. 34, pp. L24406, 2007.
38. S. Urbanski, C. Barford, S. Wofsy, C. Kucharik, E. Pyle, J. Budney, K. McKain, D. Fitzjarrald, M. Czikowsky, and J. W. Munger, "Factors controlling CO2 exchange on time scales from hourly to decadal at Harvard Forest," *Journal of Geophysical Research*, vol. 112, no. G02020, pp. doi:10.1029/2006JG000293, 2007.
39. Z.Wan and J. Dozier, "A generalized split-window algorithm for retrieving landsurface temperature from space," *IEEE Trans. Geosci. Remote Sens.*, vol. 34, pp. 892–905, 1996.
40. S. Wang, R. F. Grant, D. L. Verseghy, and T. A. Black, "Modelling plant carbon and nitrogen dynamics of a boreal aspen forest in CLASS - The Canadian Land Surface Scheme," *Ecological Modelling*, vol. 142, pp. 135–154, 2001.
41. S.Wang, R. F. Grant, D. L. Verseghy, and T. A. Black, "Modelling carbon dynamics of boreal forest ecosystems using the Canadian Land Surface Scheme," *Climatic Change*, vol. 55, pp. 451–477, 2002(a).
42. S. Wang, W. Chen, and J. Cihlar, "New calculation methods of diurnal distributions of solar radiation and its interception by canopy over complex terrain," *Ecological Modelling*, vol. 155, pp. 191–204, 2002(b).
43. S. Wang, "Dynamics of surface albedo of a boreal forest and its simulation," *Ecological Modelling*, vol. 183, pp. 477–494, 2005.
44. S. Wang and A. Davidson, "Impact of climate variations on surface albedo of a temperate grassland," *Agricultural and Forest Meteorology*, pp. 133–142, 2007.
45. R. H. Waring, N. C. Coops, W. Fan, and J. M. Nightingale, "MODIS Enhanced Vegetation Index predicts tree species richness across forested ecoregions in the contiguous U.S.A.," *Remote Sensing of Environment*, vol. 103, pp. 218–226, 2006.
46. X. Xiao, S. Boles, S. Frolking, W. Salas, B. Moore, C. Li, L. He, and R. Zhao, "Observation of flooding and rice transplanting of paddy rice fields at the site to landscape scales in China using VEGETATION sensor data," *International Journal of Remote Sensing*, vol. 23, pp. 3009–3022, 2002.
47. X. Xiao, D. Hollinger, J. D. Aber, M. Goltz, E. A. Davidson, Q. Zhang, and I. Berrien Moore, "Satellite-based modeling of gross primary production in an evergreen needleleaf forest," *Remote Sensing of Environment*, vol. 89, pp. 519–534, 2004.
48. W. Yuan, S. Liu, G. Zhou, L. L. Tieszen, D. Baldocchi, C. Bernhofer, H. Gholz, A. H. Goldstein, M. L. Goulden, D. Y. Hollinger, Y. Hu, B. E. Law, P. C. Stoy, T. Vesala, and S. C. Wofsy, "Deriving a light use efficiency model from eddy covariance flux data for predicting daily gross primary production across biomes," *Agricultural and Forest Meteorology*, vol. 143, pp. 189–207, 2007.